Geochimica et Cosmochimica Acta, Vol. 69, No. 22, pp. 5333–5349, 2005

0016-7037/05 $30.00 + .00

doi:10.1016/j.gca.2005.06.019

A model for silicate melt viscosity in the system $CaMgSi_2O_6$-$CaAl_2Si_2O_8$-$NaAlSi_3O_8$

JAMES K. RUSSELL[1,*] and DANIELE GIORDANO[1,2]

[1]Volcanology & Petrology Laboratory, Earth & Ocean Sciences, The University of British Columbia, Vancouver, British Columbia V6T 1Z4 Canada

[2]Dipartimento di Scienze Geologiche, Terza Università di Roma, Largo Leonardo Murialdo 1, 00154 Roma, Italy

(*Received February* 11, 2005; *accepted in revised form June* 22, 2005)

Abstract—Five hundred eighty-five viscosity measurements on 40 melt compositions from the ternary system $CaMgSi_2O_6$ (Di)-$CaAl_2Si_2O_8$ (An)-$NaAlSi_3O_8$ (Ab) have been compiled to create an experimental database spanning a wide range of temperatures (660–2175°C). The melts within this ternary system show near-Arrhenian to strongly non-Arrhenian properties, and in this regard are comparable to natural melts. The database is used to produce a chemical model for the compositional and temperature dependence of melt viscosity in the Di-An-Ab system. We use the Vogel-Fulcher-Tammann equation (VFT: $\log \eta = A + B/(T - C)$) to account for the temperature dependence of melt viscosity. We also assume that all silicate melts converge to a common viscosity at high temperature. Thus, A is independent of composition, and all compositional dependence resides in the parameters B and C. The best estimate for A is −5.06, which implies a high-temperature limit to viscosity of $10^{-5.06}$ Pa s. The compositional dependence of B and C is expressed by 12 coefficients ($b_{i=1,2.6}$, $c_{j=1,2..6}$) representing linear (e.g., $b_{i=1:3}$) and higher order, nonlinear (e.g., $b_{i=4:6}$) contributions. Our results suggest a near-linear compositional dependence for B (<10% nonlinear) and C (<7% nonlinear). We use the model to predict model VFT functions and to demonstrate the systematic variations in viscosity due to changes in melt composition. Despite the near linear compositional dependence of B and C, the model reproduces the pronounced nonlinearities shown by the original data, including the crossing of VFT functions for different melt compositions. We also calculate values of T_g for melts across the Di-An-Ab ternary system and show that intermediate melt compositions have T_g values that are depressed by up to 100°C relative to the end-members Di-An-Ab. Our non-Arrhenian viscosity model accurately reproduces the original database, allows for continuous variations in rheological properties, and has a demonstrated capacity for extrapolation beyond the original data.

1. INTRODUCTION

The prediction of viscosity for naturally occurring silicate melts remains one of the major challenges in petrology, volcanology, and geochemistry because of the role viscosity plays in the formation, transport, and eruption of magma (e.g., Dingwell, 1995; Spera, 2000). Previous models for forecasting the viscosity (η) of silicate melts as a function of temperature and composition have been limited by adopting a strictly Arrhenian formulation (e.g., Bottinga and Weill, 1972; Shaw, 1972; Prusevich, 1988; Persikov, 1991; Persikov, 1998) or by compositional restrictions (e.g., Baker, 1996; Hess and Dingwell, 1996). There are now published values of experimentally determined viscosities for most common silicate melt compositions and for temperature ranges pertinent to natural magmas (e.g., Dingwell, 1995; Richet and Bottinga, 1995). These data clearly demonstrate that predictive models for viscosities of natural melts must accommodate both Arrhenian and non-Arrhenian temperature dependencies (Angell, 1985; Russell et al., 2002). In this regard, the recent work by Giordano and Dingwell (2003a) is a substantial improvement over previous models (e.g., Bottinga and Weill, 1972; Shaw, 1972; Persikov, 1998) because it allows for a non-Arrhenian temperature dependence and accurately reproduces viscosities over a wide range of anhydrous, natural melt compositions.

The purpose of this paper is to present a chemical model for the non-Arrhenian temperature dependence of viscosity in the compositional system diopside ($CaMgSi_2O_6$, Di)-Anorthite ($CaAl_2Si_2O_8$, An)-Albite ($NaAlSi_3O_8$, Ab). We adopted the Vogel-Fulcher-Tammann (VFT) equation (Vogel, 1921; Fulcher, 1925; Tammann and Hesse, 1926)

$$\log\eta = A + \frac{B}{T - C} \quad (1)$$

as a purely empirical means of describing the non-Arrhenian temperature dependence of melt viscosity (Angell, 1991; Bottinga et al., 1995; Richet and Bottinga, 1995; Rossler et al., 1998). The ternary system is of general interest to geochemists because two of the end-member compositions serve as simple rheological analogues for natural basaltic (Di) and rhyolitic (Ab) melts. The system also contains melts that show a substantial range of *fragilities* (Angell, 1985), although the total range in fragility is much less than that found in molecular or organic glass-melt systems. Relative to other geologically relevant melts, the Di-An-Ab system contains strong to fragile melts showing near-Arrhenian to highly non-Arrhenian temperature dependencies, respectively.

There is an extensive database of published viscosity experiments on Di-An-Ab melts, and we use these data to solve for 13 coefficients that describe the compositional dependence of the parameters in the VFT equation (Eqn. 1). An important premise in our model is that all silicate melts converge to a common, high-temperature limiting value of viscosity (e.g., Myuller, 1955; Frenkel, 1946; Angell, 1985; Russell et al.,

* Author to whom correspondence should be addressed (krussell@eos.ubc.ca).

Table 1. Optimal model parameters (A, B, C) from fitting VFT equation to viscosity datasets for 40 individual melt compositions in the system Di-An-Ab.

Label[1]	N	ΔT (K)	Sources[2]	A	B	C	RMSE
Di	71	987–2312	a*, b, c, d, e, f, g*	−4.44	4384	728	0.13
An	67	1083–2449	d, e, g, h*, i	−4.71	5572	796	0.15
Ab	75	997–2003	e, g, h*, j, k, l	−5.35	12396	371	0.14
$Ab_{50}An_{50}$	29	1098–1860	h*, m	−4.76	7386	666	0.16
$An_{87}Ab_{9}$	4	1123–1199	m	−2.52	5486	751	0.17
$An_{82}Ab_{18}$	5	1098–1199	m	−12.08	15072	497	0.07
$Ab_{25}An_{75}$	10	1789–1875	h*	−5.97	8449	646	0.05
$Ab_{80}An_{20}$	12	1532–1874	h*	−10.42	28371	−390	0.03
$An_{61}Ab_{37}$	6	1098–1223	m	−4.17	7263	660	0.10
$An_{55}Ab_{45}$	8	1078–1258	m	−9.13	13262	474	0.05
$An_{40}Ab_{56}$	5	1073–1248	m	−3.33	7129	635	0.03
$An_{34}Ab_{62}$	6	1073–1248	m	−3.74	7858	597	0.04
$An_{30}Ab_{70}$	6	1073–1248	m	−5.97	10910	492	0.08
$Di_{10}An_{89}$	5	1100–1153	o	0.83	2920	857	0.02
$Di_{50}An_{50}$	10	1473–1873	d	−2.41	2116	976	0.01
$Di_{58}An_{42}$	9	1448–1873	d	−2.56	2273	934	0.01
$Di_{20}An_{80}$	19	1073–1873	d, i	−4.36	4926	787	0.11
$Di_{30}An_{70}$	15	1053–1873	d, o	−5.99	7036	680	0.16
$Di_{40}An_{60}$	19	1021–1873	d, i	−4.02	4451	765	0.12
$Di_{64}An_{36}$	14	1003–1773	i	−4.31	4435	749	0.12
$Di_{80}An_{20}$	19	1003–1873	d, i	−4.84	4866	720	0.14
$Di_{90}An_{10}$	6	1573–1823	d	−3.67	3930	640	0.00
$Di_{30}Ab_{70}$	9	948–1100	n	1.05	3030	692	0.07
$Di_{50}Ab_{50}$	20	933–1823	k, n	−4.76	6699	564	0.12
$Di_{95}Ab_{5}$	5	1623–1823	k	−4.64	6510	332	0.00
$Di_{84.2}Ab_{15.8}$	6	988–1074	n	−1.69	3734	707	0.01
$Di_{75}Ab_{25}$	9	1473–1863	k	−2.32	2349	868	0.01
$Di_{69.3}Ab_{30.7}$	7	947–1053	n	−0.99	3658	683	0.01
$Di_{60}Ab_{40}$	9	947–1099	n	−0.51	3518	682	0.03
$Di_{25}Ab_{75}$	10	1423–1873	k	−3.88	7505	462	0.00
$Di_{20.2}Ab_{79.8}$	10	948–1124	n	−0.44	4701	599	0.03
$Di_{9}Ab_{91}$	16	988–1223	n	−6.92	14229	260	0.05
$Di_{18.5}An_{49.8}Ab_{31.7}$	6	1020–1123	n	−1.07	4351	705	0.01
$Di_{38.3}An_{5.9}Ab_{55.8}$	9	963–1074	n	−0.21	3658	675	0.03
$Di_{55.1}An_{14.5}Ab_{30.4}$	8	963–1098	n	−2.93	5119	641	0.01
$Di_{21.2}An_{8.8}Ab_{70}$	9	963–1124	n	−2.39	6286	556	0.04
$Di_{28.2}An_{15.5}Ab_{56.3}$	8	963–1099	n	−1.61	4930	624	0.01
$Di_{35.9}An_{21.7}Ab_{42.2}$	9	966–1124	n	−1.70	4762	643	0.03
$Di_{43.8}An_{27.6}Ab_{28.6}$	7	988–1100	n	−4.09	6420	599	0.02
$Di_{51.7}An_{32}Ab_{16.3}$	8	988–1124	n	−6.86	8703	544	0.03

RMSE denotes root mean square error.

[1] Labels are reported as nominal (mol%) compositions that may not sum to 100.

[2] (a) Kirkpatrick (1974); (b) Licko & Danek (1986); (c) Neuville & Richet (1991); (d) Scarfe et al. (1983); (e) Sipp et al. (2001); (f) Sykes et al. (1993); (g) Urbain et al. (1982); (h) Cranmer & Ulhmann (1982); (i) Taniguichi (1992); (j) N'Dala et al. (1984); (k) Scarfe & Cronin (1986); (l) Stein & Spera (1993); (m) Hummel & Arndt (1985); (n) Tauber (1987); (o) Tauber & Arndt (1987); *low-temperature experiments not used.

2002; Russell et al., 2003). This assumption requires the parameter A to be a constant, independent of melt composition; compositional dependence is accommodated solely by variations in B and C terms. The main attributes of the chemical model are that it reproduces the original data to within experimental error, captures the full range of rheological behaviour observed in the system Di-An-Ab, and can predict smooth, continuous transitions in rheology (e.g., strongly non-Arrhenian to near-Arrhenian) as a function of changes in melt composition.

2. THE DATA SET

One of the benefits of working on a classic system such as the Di-An-Ab ternary system is that there is a wealth of experimental data. Viscosity measurements have been published for melts that span the full compositional range of the system and for wide ranges of temperature. Our original compilation considered more than 825 viscosity measurements deriving from experiments on 53 different melt compositions. The number of measurements associated with each melt composition varies substantially; most of the data are for the end-member and binary compositions.

Not all of the published data were used in the model. Melts in the Di-An-Ab system comprise the oxide components SiO_2, Al_2O_3, MgO, CaO, and Na_2O; however, we only considered viscosity data for melts having strictly ternary compositions (+/-2 mol%). We elected to drop experimental data from some of the early pioneering papers (e.g., Kozu and Kani, 1935; Machin et al., 1952; Machin et al., 1954) where there was no independent analysis of the nominal melt composition (i.e., electron microprobe analysis), or the reported uncertainties on the viscosity data were excessive ($> \pm 0.5$ log units). In several

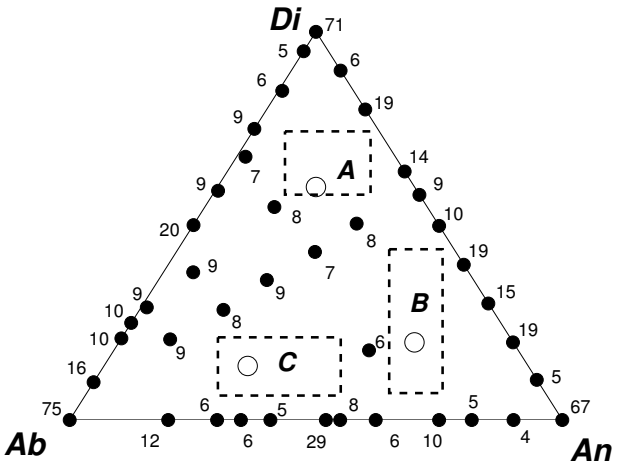

Fig. 1. Ternary diagram Di-An-Ab shows the range of melt compositions in the experimental database and the total number of viscosity measurements at each melt composition. The data set used for modeling was restricted to 40 compositions and 585 experiments (Table 1). Dashed boxes denote compositional domains where data are absent or sparse. Letters denote melt compositions from the literature that are used below: (A) $Di_{60}An_{20}Ab_{20}$, (B) $Di_{20}An_{60}Ab_{20}$, and (C) $Di_{13.1}An_{30.6}Ab_{54.3}$.

cases we benefited from having multiple data sets of viscosity for the same melt composition and over the same range of temperatures. If there were discrepancies between the two data sets, we adopted the more recent data, believing them to be more precise and the melt compositions to be better characterized (e.g., An_{100}; Sipp et al. [2001] vs. Hummel and Arndt [1985]; Table 1). We also rejected experiments where partial crystallization occurred (or was suspected) during the measurement procedure (Kozu and Kani, 1935; Machin et al., 1952). Our analysis also excluded all viscosity measurements made at elevated (>1 atm) confining pressures or in the presence of H_2O (e.g., Kushiro, 1978; Brearley et al., 1986; Taniguchi, 1992; Schulze et al., 1999). The selection process left us with 585 viscosity: T(K) data points collected on 40 different melt compositions (Fig. 1; Table 1). The data are evenly distributed along the binaries but are relatively sparse within the ternary (N = 8). The data span a temperature range of 660 to 2175°C and values of log η range from −1.25 to 14.5 Pa s (Fig. 2A).

The main problems encountered in the data compilation exercise concerned the compositions of the experimental melts and included (a) a lack of independent chemical analysis or relatively poor (<100%) analysis of the experimental materials (Kozu and Kani, 1935; Machin et al., 1952; Machin et al.,1954), (b) substantial discrepancies between the nominal and measured compositions, and (c) nonstoichiometric melt compositions that lie outside of the true ternary system (e.g., Machin et al., 1952; Machin et al., 1954). Consequently, all compositions were converted to mole fractions of Di, An, and Ab from the mole fractions of the oxides (e.g., X_{Al2O3}) using the following sequence of calculations: (i) $X_{Di} = 4\ X_{MgO}$; (ii) $X_{An} = 4\ X_{CaO} - X_{Di}$; and (iii) $X_{Ab} = 8\ X_{Al2O3} - 2\ X_{An}$ or $X_{Ab} = 8\ X_{Na2O}$. The Ab component was computed using both Al_2O_3 and Na_2O contents, which provided an independent check on melt composition. Ideally, the two methods returned equivalent values. If the two values were in close agreement, we accepted the representation that provided a total closest to 100 mol%. Where the differences were >4 mol%, we dropped the data from further consideration; such discrepancies usually indicated a loss of Na_2O. The recalculated normalized melt compositions are reported as mole fractions of Di, An, and Ab in Table 2.

As the data were compiled and evaluated, we made every attempt to assess and assign experimental uncertainties (i.e., 1 σ) to the viscosity measurements. These estimates derive from the original publication or from our analysis of the dispersion in the original experimental data. Values of log η were assigned values for 1 σ uncertainties on log η of 0.15 to 0.25.

3. VFT FUNCTIONS AND INDIVIDUAL DATA SETS

The VFT equation (Eqn. 1) has three adjustable parameters that accommodate the temperature dependence of melt viscosity, and they are expected to vary for different melt compositions (e.g., Richet and Bottinga, 1995; Hess et al., 1996). The parameter A is the value of log η (Pa s) at infinite temperature, and C is the temperature (K) at which viscosity becomes infinite. The parameter B (units of K) is proportional to the activation energy associated with viscous flow and represents the potential energy barrier obstructing the structural rearrangement of the melt. We anticipate that these parameters have different degrees and forms of compositional dependence.

To provide a baseline for future comparisons, we begin by fitting the VFT equation to the experimental data for each of the 40 different melt compositions (Fig. 1; Table 1). The optimal parameters (A, B, and C) for the VFT equation are obtained for each melt composition by minimization of the χ^2 function:

$$\chi^2 = \sum_{i=1}^{n} \left[\frac{\log \eta_i - \left[A + \frac{B}{T - C} \right]}{\sigma_i} \right]^2 \qquad (2)$$

where n is the number of experimental observations [log η_i:T_i] for each melt composition, and σ_i denotes the experimental uncertainty on each measurement of log η (cf. Press et al., 1986; Russell et al., 2003).

The model parameters for each melt composition are reported in Table 1. We also report the root mean square error (RMSE) for each optimization as a relative measure of fit quality (Press et al., 1986). How well the model curves describe the data is purely a reflection of the quality of the viscosity measurements (e.g., precision and accuracy) and the distribution (Δlog η:ΔT) of the data. The optimized VFT functions reproduce most of the experimental data to within ±0.25 log η (Fig. 2B). Furthermore, the residuals are evenly distributed across the full range of viscosities (Fig. 2B). Also shown in Figure 2 are the model parameters obtained for each of the 40 melt compositions: A (-12–1), B (2,000–28,400), and C (-390–976). The range of model parameters found for the entire suite of melt compositions is substantially larger than the range defined by the end-member melts (Di, An, and Ab). The solution space bounded by the end-member melts encloses very few of the binary and ternary melts (Fig. 2C,D).

Several of the fits produce physically unrealistic solutions (Fig. 2C,D, grey shaded fields) corresponding to values of A >0 and values of C <0 K. The three melt compositions associated with these unphysical solutions (Table 1) are

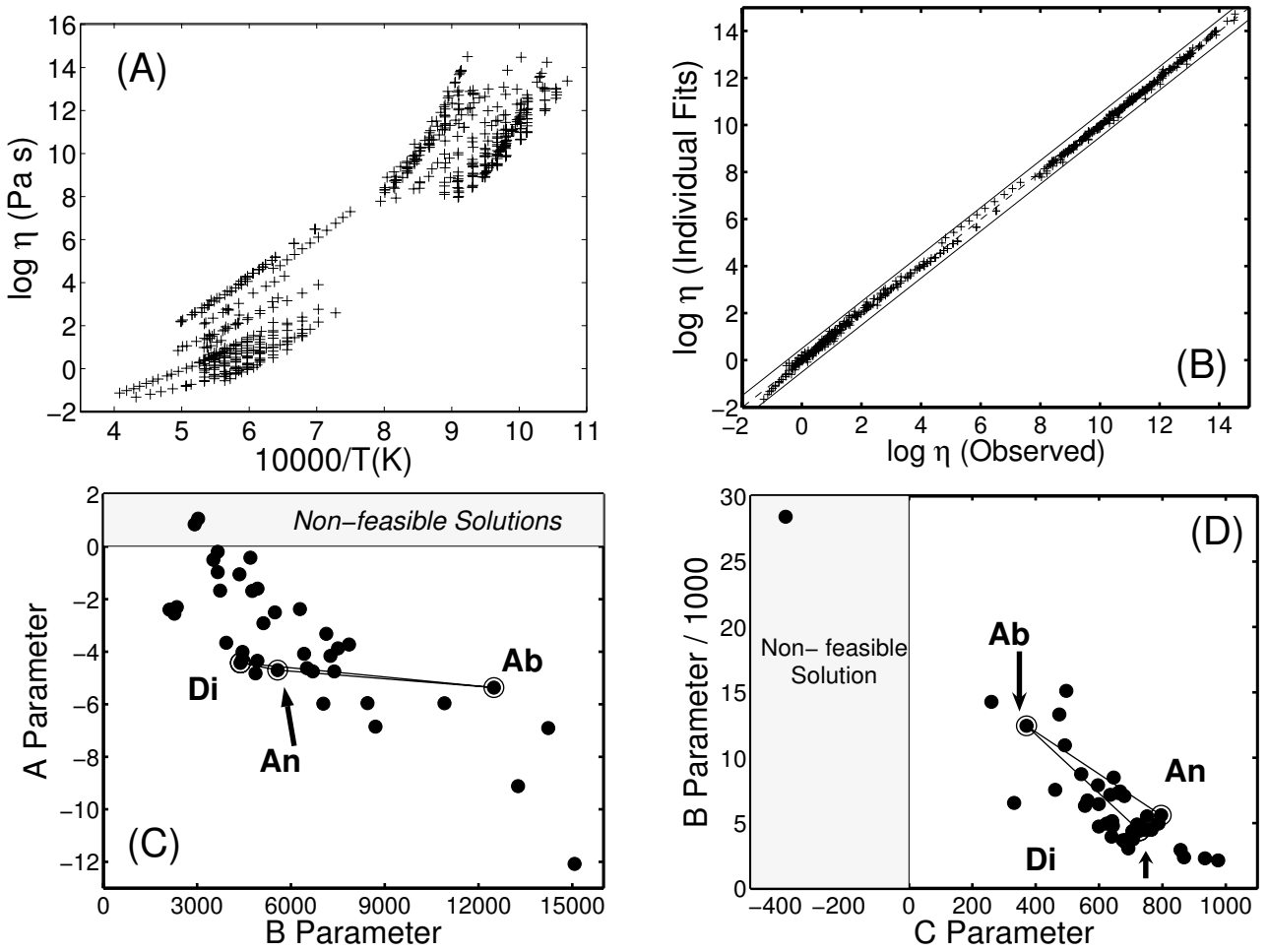

Fig. 2. Results of fitting the VFT function to individual viscosity data sets compiled for each melt composition (Table 1). (A) The entire data set plotted as log η (-1.3–14.5) vs. reciprocal T(K) (920–2450 K). (B) Values of log η predicted by model VFT functions compared to original data; dashed lines denote ± 0.5 log units of viscosity. Values of adjustable parameters (e.g., A, B, C) by fitting VFT equation to individual data sets are plotted as (C) A vs. B, and (D) B/1000 vs. C. Parameters for $Ab_{80}An_{20}$ plot off-scale of abscissa axis. End members (e.g., Di, An, Ab) are indicated by large open circles joined by solid lines. Grey shaded boxes denote solution space that is physically unreasonable.

$An_{20}Ab_{80}$, (C = −390), $Di_{10}An_{89}$ (A = 0.83), and $Di_{30}Ab_{70}$ (A = 1.05). The value of B obtained for $An_{20}Ab_{80}$ (e.g., B = 28,400; Table 1) is also somewhat suspect. To a first approximation, values of B relate to the "degree of polymerization," and hence, to the average bond strength of the silicate network. On this basis one would expect the highest value of B to correspond to Ab melts (B_{Ab} = 12,396) and not to an intermediate compound.

To a large extent, these physically unrealistic solutions result because there are too few data or the data do not span a large enough viscosity range to uniquely constrain the adjustable parameters A, B, and C. For example, the two data sets for $Di_{10}An_{89}$ and $Di_{30}Ab_{70}$ are sparse, cover a small range of temperatures (<150°C), and include only high viscosity data (η = 10^9 - 10^{13} Pa s). Consequently, the high-temperature limits, as represented by the parameter A, are only weakly constrained. Similarly, the value of C (low-T limiting behaviour) obtained for $An_{20}Ab_{80}$ melts has large uncertainties because, although there are more (N = 12) experimental data, they cover only low viscosity (e.g., η = 10^2 - 10^4 Pa s) measurements. If we momentarily drop the three nonfeasible fits from consideration, the range of model parameters (e.g., A, B, and C) for the 40 melt compositions is substantially reduced (A: −12 to −0.5; B: 2000 to 15,070; C: 260 to 976).

4. THE CONSTANT "A" CONCEPT

Fitting the VFT function to individual viscosity data sets does not necessarily lead to unique values of the model parameters A, B, and C (Russell et al., 2002). Even where the experimental data span a wide range of viscosity values (e.g., 10^2–10^{12} Pa s), there are multiple combinations of values of A, B, and C that can describe the data equally well. Stated another way, many viscosity data sets do not uniquely constrain the values of the VFT parameters. Indeed, our previous modeling of data for the end-member melt compositions Di-An-Ab demonstrated that all three melts could be modeled with a common

Table 2. Model parameters B and C derived from simultaneous fitting VFT functions to the global dataset and solving for a common value of A (−4.62 ± 0.66 (95% cl)). Melt compositions have been recalculated, normalized, and reported as mol% of Dp, An, and Ab (see text).

Label	Di	An	Ab	NBO/T	B	C	RMSE
Di	1.00	0.00	0.00	2	4577	719	0.13
An	0.00	1.00	0.00	0	5452	801	0.15
Ab	0.00	0.00	1.00	0	10950	427	0.14
$Ab_{50}An_{50}$	0.00	0.50	0.50	0	7160	677	0.17
$An_{87}Ab_{9}$	0.00	0.90	0.10	0	7330	688	0.17
$An_{82}Ab_{18}$	0.00	0.82	0.18	0	6931	705	0.07
$Ab_{25}An_{75}$	0.00	0.75	0.25	0	6401	733	0.12
$Ab_{80}An_{20}$	0.00	0.20	0.80	0	9330	495	0.04
$An_{61}Ab_{37}$	0.00	0.62	0.38	0	7711	645	0.11
$An_{55}Ab_{45}$	0.00	0.55	0.45	0	7815	632	0.07
$An_{40}Ab_{56}$	0.00	0.41	0.59	0	8525	588	0.03
$An_{34}Ab_{62}$	0.00	0.35	0.65	0	8862	562	0.04
$An_{30}Ab_{70}$	0.00	0.30	0.70	0	9187	546	0.08
$Di_{10}An_{89}$	0.10	0.90	0.00	0.105	6565	724	0.03
$Di_{50}An_{50}$	0.50	0.50	0.00	0.667	6079	521	0.04
$Di_{58}An_{42}$	0.58	0.42	0.00	0.817	5997	513	0.04
$Di_{20}An_{80}$	0.20	0.80	0.00	0.222	5238	773	0.12
$Di_{30}An_{70}$	0.30	0.70	0.00	0.353	5242	757	0.21
$Di_{40}An_{60}$	0.40	0.60	0.00	0.500	5152	733	0.13
$Di_{64}An_{36}$	0.64	0.36	0.00	0.941	4752	734	0.12
$Di_{80}An_{20}$	0.80	0.20	0.00	1.333	4611	732	0.14
$Di_{90}An_{10}$	0.90	0.10	0.00	1.636	6163	376	0.00
$Di_{30}Ab_{70}$	0.29	0.01	0.70	0.339	7739	504	0.10
$Di_{50}Ab_{50}$	0.50	0.00	0.50	0.667	6502	572	0.12
$Di_{95}Ab_{5}$	0.95	0.00	0.05	1.810	6446	339	0.00
$Di_{84.2}Ab_{15.8}$	0.85	0.01	0.14	1.478	5838	628	0.02
$Di_{75}Ab_{25}$	0.75	0.00	0.25	1.200	7276	287	0.03
$Di_{69.3}Ab_{30.7}$	0.68	0.02	0.30	1.030	6263	588	0.03
$Di_{60}Ab_{40}$	0.59	0.01	0.40	0.837	6735	558	0.07
$Di_{25}Ab_{75}$	0.25	0.00	0.75	0.286	9295	332	0.01
$Di_{20.2}Ab_{79.8}$	0.21	0.00	0.79	0.235	8925	440	0.05
$Di_{9}Ab_{91}$	0.10	0.00	0.90	0.105	10662	371	0.06
$Di_{18.5}An_{49.8}Ab_{31.7}$	0.18	0.52	0.30	0.198	7293	600	0.03
$Di_{38.3}An_{5.9}Ab_{55.8}$	0.38	0.06	0.56	0.469	7228	539	0.04
$Di_{55.1}An_{14.5}Ab_{30.4}$	0.55	0.14	0.31	0.759	6489	594	0.02
$Di_{21.2}An_{8.8}Ab_{70}$	0.21	0.10	0.69	0.235	8601	475	0.05
$Di_{28.2}An_{15.5}Ab_{56.3}$	0.28	0.17	0.55	0.326	7619	528	0.03
$Di_{35.9}An_{21.7}Ab_{42.2}$	0.36	0.22	0.42	0.439	7322	550	0.04
$Di_{43.8}An_{27.6}Ab_{28.6}$	0.43	0.28	0.29	0.548	6887	584	0.02
$Di_{51.7}An_{32}Ab_{16.3}$	0.51	0.33	0.16	0.685	6585	609	0.04

value of A implying a common viscosity (e.g., $\eta_\infty = 10^{-4.5\pm0.4}$) at high T (Russell et al., 2002; Russell et al., 2003).

4.1. Constant "A" and Ternary Melt Compositions

We have used a similar approach to fit VFT functions to the data for all 40 melt compositions simultaneously. Specifically, each melt composition is allowed a unique value of B and C, but the optimization requires that all of the melts share a common, but unknown, value of A. This approach reduces the total number of adjustable parameters from 3*N (e.g., 120; Table 1) to 2*N + 1 (81, Table 2). The solution is obtained by minimization of the function:

$$\chi^2 = \sum_{j=1}^{N}\sum_{i=1}^{m_j}\left[\frac{\log\eta_{ij} - \left[A + \frac{B_j}{T_{i,j} - C_j}\right]}{\sigma_{i,j}}\right]^2 \quad (3)$$

where j is the index for each melt composition, i is the index for each of m_j experiments in the j^{th} data set and $\eta_{i,j}$, $T_{i,j}$ and $\sigma_{i,j}$ are the corresponding data. The solution returns a single value for A and N and different values for B_j and for C_j.

The results of the global optimization are summarized in Table 2 and Figure 3. The optimization reproduces virtually all of the original data to within 0.5 log units, and the residuals between model and experiment are randomly distributed (i.e., no correlation with log η; Fig. 3A). There is also very little degradation in the quality of the fits of VFT functions to each melt composition based on the corresponding RMSE (Table 2). The inset to Figure 3A directly compares the residuals arising from the fits to individual melt compositions (Table 1) to the residuals deriving from the constant A optimization (Table 2). There is essentially no difference, despite the fact that the latter optimization uses 39 fewer adjustable parameters.

The optimization returns an estimate on A of −4.62 +/- 0.66 (95%), representing a common high-temperature limiting value for silicate melt viscosity (e.g., $10^{-4.6}$ Pa s). The optimal values of B and C for all melt compositions are plotted in Figure 3B. The range of values of B (4570–10950)

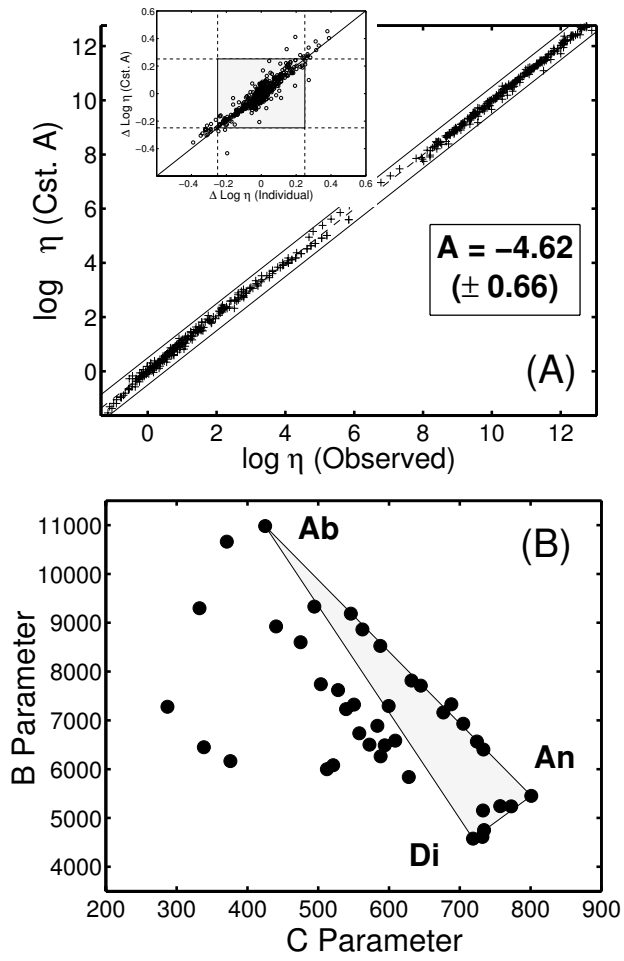

Fig. 3. Results of simultaneously fitting VFT functions to entire viscosity data set for unique values of B and C and a common value for A (Table 2). (A) Values of log η predicted by model VFT functions compared to original data; dashed lines denote ±0.5 log units of viscosity. Inset compares residuals (model observed) due to fitting each data set independently vs. fitting them simultaneously for a constant value of A. (B) Optimal values of B and C associated with the constant A model.

and C (287–801) is considerably smaller than that achieved by fitting each composition independently. This is because the common A assumption causes strong coupling between all of the adjustable parameters. This coupling lends stability to the optimization and actually reduces the range of B and C values that can be chosen to describe the experimental data sets.

In the situation where the data for an individual melt composition are few, or only cover a small range of temperature, the optimal parameters from the constant A model can be quite different (cf. $An_{55}Ab_{45}$ in Table 1 vs. Table 2). Conversely, the optimal values of B and C for compositions having a wide range of viscosity data tend not to change appreciably. For example, the model curves for the three end members, based on a common value of A, have values of B and C (Table 2), similar to those obtained by fitting each data set independently (Table 1): Di (4577 and 719 vs. 4384 and 728), An (5452 and 801 vs. 5572 and 796), and Ab (10950 and 427 vs. 12396 and 371). The values of B and C for the end-member melts (Di, An, Ab) now enclose many of the parameter values obtained for the binary and ternary melt compositions (Fig. 3B). The maximum value of B is ascribed to the most polymerized composition, Ab (10,950), and the minimum to Di (4577), which is the least polymerized melt. The An end member defines the maximum in C (801), whereas the minimum in C (287) comes from the composition $Di_{75}Ab_{25}$. The model values for Ab-An melts lie essentially along the binary join defined by the end members. This is also true for Di-An melts. Melts along the binary Di-Ab or ternary melts lie outside of the field bounded by the three end members.

In summary, the optimization based on a common, but unknown, value of A for all ternary melts accurately reproduces the experimental data (Fig. 3A). This optimization has two additional attributes. Firstly, forcing the melts to converge to a common value of viscosity at high temperature induces a strong coupling between data sets that stabilizes the range of solutions for small data sets (e.g., $An_{82}Ab_{18}$; Table 1; Table 2). Secondly, the optimization provides our best experimental estimate of the high-temperature limits to silicate melt viscosity (e.g., $10^{-4.6}$ Pa s), which accord with the range of values suggested by theory (e.g., Myuller, 1955; Frenkel, 1959; Angell, 1985; Toplis, 1998; Russell et al., 2003).

5. A CHEMICAL MODEL

Below we develop a compositional model for the non-Arrhenian temperature dependence of melt viscosity in the system Di-An-Ab. The value A is treated as independent of composition, but unknown. The parameters B and C are

Table 3. Multicomponent model for temperature and compositional dependence of melt viscosity in system Di-An-Ab. Data are fit simultaneously to the VFT equation for a constant value of A (−5.06 ± 0.3) and compositional coefficients for the B and C terms. Confidence limits (95%) on model parameters are also reported in brackets.

	B Coefficients			C Coefficients		
	Di	An	Ab	Di	An	Ab
Di	5092 (415)	–	–	696 (21)	–	–
An	−377 (910)	6070 (438)	–	−84.8 (60)	775 (20)	–
Ab	−3091 (1733)	−2960 (1624)	11890 (701)	−150 (114)	166 (106)	373 (33)
χ^2			1469 (Average 36.7)			
RMSE			0.3			

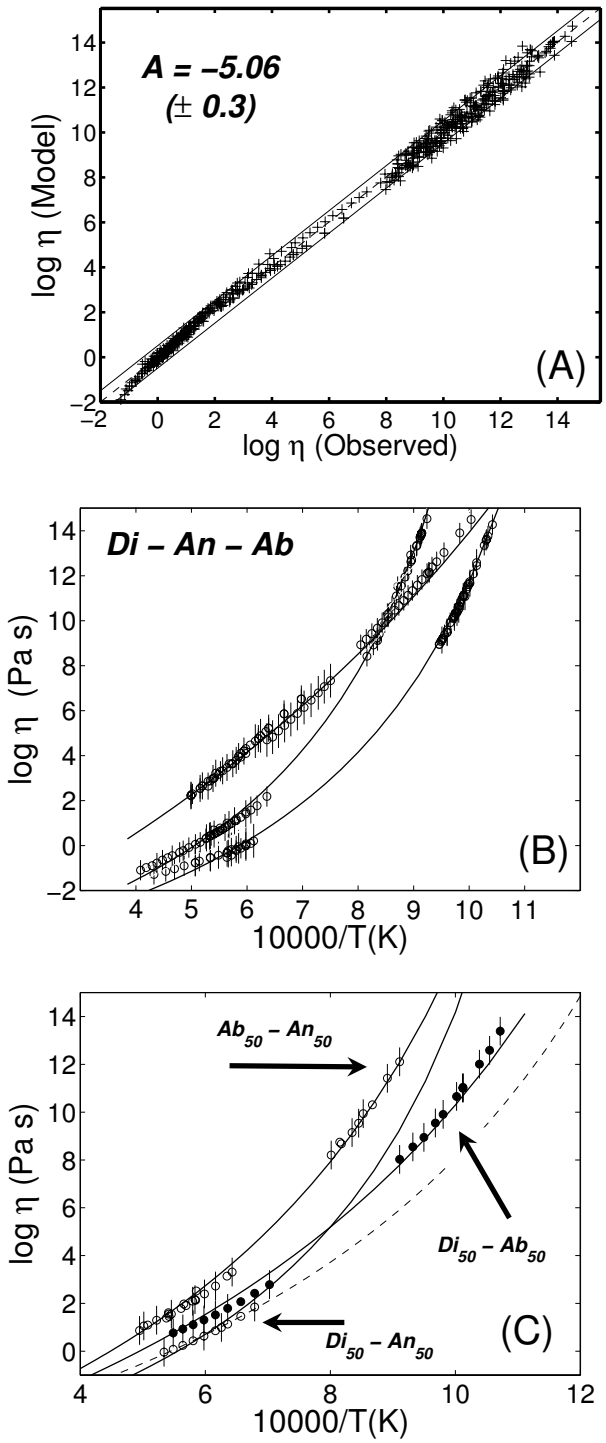

Fig. 4. Multicomponent model for temperature-dependent melt viscosity in system Di-An-Ab (Table 3). (A) Values of log η predicted by multicomponent melt model compared to original data; dashed lines denote ±0.5 log units of viscosity. (B) Model VFT curves (solid lines) predicted by multicomponent model compared to original data for end-member melt compositions (Di, An, and Ab), and (C) for the midpoint compositions of the binaries Di-An, Di-Ab, and Ab-An. Dashed line shows previous fit to $Di_{50}An_{50}$ data set (Table 2). Vertical bars denote 3 σ uncertainties on experimental data.

assumed to have a compositional dependence on the mole fractions of melt components (x_i) given by

$$B = b_1x_1 + b_2x_2 + b_3x_3 + b_{1,2}x_1x_2 + b_{1,3}x_1x_3 + b_{2,3}x_2x_3 \quad (4)$$

and

$$C = c_1x_1 + c_2x_2 + c_3x_3 + c_{1,2}x_1x_2 + c_{1,3}x_1x_3 + c_{2,3}x_2x_3 \quad (5)$$

where the subscripts 1, 2, and 3 refer to the end-member components Di, An, and Ab, respectively. The first three terms in Eqns. 4 and 5 represent a purely linear dependence of B and C on melt composition; the last three coefficients are nonlinear, allowing for the possibility of higher order interactions between end-member components. In total there are 13 model parameters including A, b_{Di}, b_{An}, b_{Ab}, $b_{Di,An}$, $b_{Di,Ab}$, $b_{An,Ab}$, c_{Di}, c_{An}, c_{Ab}, $c_{Di,An}$, $c_{Di,Ab}$, and $c_{An,Ab}$ (Table 3). The optimization problem is linear in the unknowns (e.g., b_i, $b_{i,j}$, c_i, and $c_{i,j}$) and solved via minimization of

$$\chi^2 = \sum_{i=1}^{n}\left[\log\eta_i - \left(\frac{A + (b_{Dp}x_{Dp,i} + b_{An}x_{An,i} + b_{An,Ab}x_{An}x_{ab})}{T_i - (c_{Dp}x_{Dp,i} + c_{An}x_{An,i} + b_{An,Ab}x_{An}x_{ab})}\right)\right]^2 \quad (6)$$

where the summation is over all n experiments (e.g., 585) and each data array includes values of log η_i, T_i and $x_{Di,i}$, $x_{An,i}$, and $x_{Ab,i}$. The values of the 13 model coefficients are reported in Table 3 with their corresponding confidence limits. All values are significant at the 95% confidence level, except for the term $b_{Di,An}$ representing possible higher order interactions between Di and An on the B parameter. The implication is that interactions between Di and An are purely linear; however, for simplicity we have elected to leave this term in the model.

The accuracy of the model is summarized in Figure 4, which shows the distribution of residuals and the predicted VFT functions for 6 of the 40 melt compositions in the original database. The multicomponent chemical model reproduces most of the original data to within 0.5 log units (Fig. 4A), although the deviations at higher values of viscosity (10^8 - 10^{14} Pa s) are larger than observed in Figures 2B and 3A. It is important to realize that the chemical model (Table 3) explicitly incorporates the effects of both melt composition and temperature on viscosity whilst using many fewer adjustable parameters (13 vs. 81). In contrast, the previous model VFT functions (Tables 1 or 2) depended only on the quality of the viscosity measurements (e.g., precision and accuracy) and the distribution ($\Delta\log\eta$:ΔT) of the data. The ability of the chemical model to reproduce the original data (Fig. 4A) is excellent given these considerations and the inherent uncertainty in the compositions of many of the experimental melts.

The multicomponent model generates VFT functions that accurately reproduce the data for the end-member compositions (Fig. 4B) and for the 50:50 compositions on the binaries Di-An, Di-Ab, and Ab-An. One of these melt compositions ($Di_{50}An_{50}$) is characterized only by high-temperature data, yet our model reproduces those data well (Fig. 4C). Our predicted VFT function for this composition (solid line) is substantially different from that obtained by fitting that composition independently (Fig. 4C, dashed line; Table 1). The VFT curve derived from our chemical model is much more consistent with the pattern of data derived from other melt compositions on the Di-An binary.

Table 4. Values of B and C calculated for experimental melt compositions using multicomponent model (e.g., Table 3). Also reported are calculated values of Tg and fragility indices (see text).

Label	B	C	χ^2	RMSE	T_g[1]	F_D[2]	F_m[3]	$F_{1/2}$[4]
Di	5092	696	87	0.18	995	0.70	56.9	0.54
An	6070	775	73	0.17	1131	0.69	54.2	0.52
Ab	11890	373	155	0.23	1070	0.35	26.2	0.21
$Ab_{50}An_{50}$	8125	624	28	0.20	1100	0.57	39.4	0.40
$An_{87}Ab_{9}$	6382	750	21	0.46	1124	0.67	51.3	0.50
$An_{82}Ab_{18}$	6696	726	6	0.23	1119	0.65	48.6	0.48
$Ab_{25}An_{75}$	6970	706	4	0.13	1115	0.63	46.5	0.46
$Ab_{80}An_{20}$	10253	480	15	0.23	1081	0.44	30.7	0.29
$An_{61}Ab_{37}$	7578	662	7	0.22	1106	0.60	42.5	0.43
$An_{55}Ab_{45}$	7962	635	2	0.10	1102	0.58	40.3	0.40
$An_{40}Ab_{56}$	8804	577	7	0.23	1093	0.53	36.1	0.36
$An_{34}Ab_{62}$	9196	551	5	0.19	1090	0.51	34.5	0.34
$An_{30}Ab_{70}$	9527	528	17	0.33	1087	0.49	33.2	0.32
$Di_{10}An_{89}$	5934	759	44	0.59	1107	0.69	54.3	0.52
$Di_{50}An_{50}$	5487	715	10	0.20	1036	0.69	55.0	0.53
$Di_{58}An_{42}$	5411	709	12	0.23	1026	0.69	55.2	0.53
$Di_{20}An_{80}$	5814	746	12	0.14	1087	0.69	54.4	0.52
$Di_{30}An_{70}$	5697	734	21	0.24	1068	0.69	54.5	0.52
$Di_{40}An_{60}$	5588	723	50	0.25	1051	0.69	54.7	0.52
$Di_{64}An_{36}$	5357	705	17	0.17	1019	0.69	55.4	0.53
$Di_{80}An_{20}$	5227	699	16	0.16	1005	0.70	56.0	0.53
$Di_{90}An_{10}$	5156	697	4	0.16	999	0.70	56.4	0.54
$Di_{30}Ab_{70}$	9200	442	55	0.49	982	0.45	31.1	0.29
$Di_{50}Ab_{50}$	7701	498	59	0.34	950	0.52	35.9	0.36
$Di_{95}Ab_{5}$	5285	673	2	0.12	983	0.68	54.1	0.52
$Di_{84.2}Ab_{15.8}$	5697	632	66	0.66	966	0.65	49.3	0.49
$Di_{75}Ab_{25}$	6212	588	11	0.22	952	0.62	44.6	0.45
$Di_{69.3}Ab_{30.7}$	6517	569	53	0.55	951	0.60	42.5	0.43
$Di_{60}Ab_{40}$	7096	531	66	0.54	947	0.56	38.8	0.39
$Di_{25}Ab_{75}$	9611	426	43	0.42	989	0.43	30.0	0.27
$Di_{20.2}Ab_{79.8}$	9950	416	100	0.63	999	0.42	29.2	0.26
$Di_{9}Ab_{91}$	10957	391	82	0.45	1034	0.38	27.5	0.23
$Di_{18.5}An_{49.8}Ab_{31.7}$	6989	650	89	0.77	1059	0.61	44.1	0.44
$Di_{38.3}An_{5.9}Ab_{55.8}$	8184	492	1	0.08	972	0.51	34.6	0.34
$Di_{55.1}An_{14.5}Ab_{30.4}$	6654	583	43	0.46	973	0.60	42.5	0.43
$Di_{21.2}An_{8.8}Ab_{70}$	9238	469	62	0.52	1010	0.46	31.8	0.30
$Di_{28.2}An_{15.5}Ab_{56.3}$	8198	522	53	0.52	1002	0.52	35.6	0.35
$Di_{35.9}An_{21.7}Ab_{42.2}$	7388	564	8	0.19	997	0.57	39.3	0.39
$Di_{43.8}An_{27.6}Ab_{28.6}$	6642	611	3	0.12	1000	0.61	43.8	0.44
$Di_{51.7}An_{32}Ab_{16.3}$	6052	652	12	0.24	1006	0.65	48.4	0.48

[1] T_g values are temperatures at which melt has a viscosity of 10^{12} Pa s; Fragility indices include: [2] fragility (F_D); [3] steepness index (F_m); [4] kinetic fragility ($F_{1/2}$) (see text for definitions).

The optimal value for A is -5.06 ± 0.3 ($\eta_0 = 10^{-5.1\pm0.3}$ Pa s), which agrees well with the high-temperature limit in viscosity of $10^{-4.5\pm1}$ Pa s suggested by theoretical considerations (e.g., Glasstone et al., 1941; Frenkel, 1946; Myuller, 1955). For example, a high-T limit to silicate melt viscosity is suggested by considering the timescales of relaxation processes in melts (Angell, 1991; Richet and Bottinga, 1995; Angell et al., 2000). The Maxwell relationship ($\tau = \eta/G_\infty$) constrains the lower limits to melt viscosity. Using $\sim 10^{10}$ Pa for the bulk shear modulus (G_∞) of melt at infinite frequency and a relaxation timescale (τ) of the melt limited by the quasi-lattice vibration period ($\sim 10^{-14}$ s), the lower limiting value to viscosity (η_∞) should approximate $10^{-4\pm1}$ Pa s (Dingwell and Webb, 1989; Angell, 1991; Toplis, 1998; Angell et al., 2000). Our estimate of the high-T limit to melt viscosity ($10^{-5.06\pm0.3}$ Pa s) is also in excellent agreement with experimental observations on low-T glass-forming systems (e.g., Angell, 1991; Angell et al., 2000). These studies suggest that, at temperatures well above T_g, both strong and fragile melts commonly converge to a common viscosity of 10^{-5} Pa s (e.g., Angell, 1991; Angell et al., 2000).

The predicted values of B and C for all 40 melt compositions are reported in Table 4 and their covariation shown in Figure 5. The properties of the end-member melt compositions define a field that captures the B and C values for all binary and ternary melt compositions. The B and C parameters vary nearly linearly along the Ab-An and Di-An joins; compositions between Ab and Di show a slightly nonlinear relationship between B and C.

6. DISCUSSION

6.1. Compositional Dependence of B and C

The exact nature of the compositional dependence of B and C is portrayed explicitly by plotting them against x_{Di} and x_{Ab} (Fig. 6). The value of B changes almost linearly with increasing x_{Di} along the Di-An join (Fig. 6A) as is suggested by the

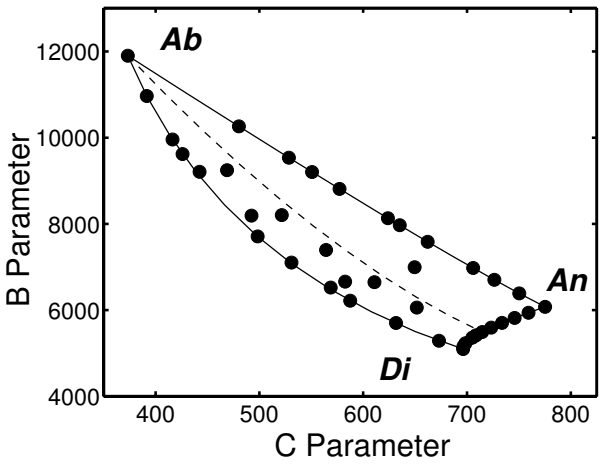

Fig. 5. Values of B and C predicted by multicomponent model for VFT functions in system Di-An-Ab. Solid circles denote values of B and C computed for experimental melt compositions (Table 4) used in calibration of the model. Values of B and C are also calculated for binary compositions (solid lines) and for melt compositions $Di_xAn_xAb_{1-2x}$ (dashed line).

confidence limits on the value of $b_{Di\text{-}An}$ (Table 3). The variations in B with increasing x_{Di} become increasingly nonlinear at higher Ab contents (Fig. 6A,B). The variations in B along the Di-Ab join is slightly more nonlinear than the variations observed along the An-Ab binary (cf. Table 3).

Values of C along the Di-An and Di-Ab joins vary nonlinearly with composition, although the departure from linearity for Di-An is slight (Fig. 6C). Plotted against x_{Ab}, model values of C decrease nonlinearly with increasing x_{Ab} content to form a convex lenslike pattern (Fig. 6D). Along the Di-Ab join, there is a negative component to the nonlinearity (concave up curve), whereas the An-Di join contains a positive nonlinear contribution (concave down curve). However, values of C decrease nearly linearly with increasing x_{Ab} for melts along the join $Di_xAn_xAb_{2x}$ as indicated by the dashed lines in Figure 6C,D.

The nature of the model dictates that values of B and C for all binary and ternary melts must be bounded by the properties of the end-member melts (e.g., Di, An, Ab). A level of self-consistency is demonstrated by the fact that calculated values of B and C for all melts in the database plot coherently along the appropriate binary join or within the field enclosed by the end-member melts. We also plotted the calculated values of B and C for each melt against the corresponding values of NBO/T (Mysen, 1986; Mysen et al., 1982; Table 2; Fig. 6E,F). The range of NBO/T in this system is from 0 (An, Ab) to 2 (Di). Model values of B show a strongly nonlinear relationship against NBO/T for binary melt compositions. The pattern shown in Figure 6E echoes that seen in Figure 6A, although the nonlinearity is more pronounced. Calculated values of C show a much simpler relationship with NBO/T (Fig. 6F) that is also sympathetic with the pattern observed between C and x_{Di} (Fig. 6C). The trends observed between calculated values of B and C and corresponding NBO/T values suggest that, although it does not capture the full compositional dependencies of B and C, NBO/T could serve as a proxy for x_{Di}.

The compositional dependence of B and C are summarized in a series of contoured ternary plots (Fig. 7). The lowest values of B reside in Di (5092 K) and An (6070 K); Ab (11890 K) has the highest value (Fig. 7A). Contours of B are nearly parallel to Di-An, indicating that values of B increase gradually and smoothly from Di-An towards Ab. Contours of C show a gradual increase from Ab (373 K), to Di (696 K), to An (775) (Fig. 7B). Along the three binary joins, the largest variations are between the Ab end member and An (Δ = 402) or Di (Δ = 323), whereas between Di and An there is only a slight change (Δ = 79).

We have also portrayed the nonlinear component of the B and C parameters as a function of composition. The contours used in Figure 7C,D show the nonlinear components of B and C as a percentage of the absolute values reported in Table 4. For example, our model requires the end-member melt compositions to lie on the 0% contour. Contours for the B parameter show a near-linear compositional dependence along the Di-An join (Table 3; Fig. 6A). The maximum nonlinear contribution to values of B is ~10% and coincides with compositions along the join $Di_{60}Ab_{40}$-$An_{60}Ab_{40}$ (e.g., $x_{Ab} \cong 0.5$). The nonlinear component to C appears more complicated, although most of the ternary system shows $<\pm 3\%$ departure from a strictly linear compositional dependence. The largest departures from linearity are along the Di-Ab (-7%) and An-Ab (+6%) joins (cf. Table 3; Fig. 6D). Some of the apparent complexity in the contour patterns of the nonlinear contributions to B (Fig. 7C) and C (Fig. 7D) could result from gaps in the data. We do not consider this an issue where the contours are smooth and regular in geometry. However, there may be less confidence in domains where the contours show relatively pronounced changes in behaviour and there are no data. Fortunately for our description of the compositional dependence of C, the least constrained portion of the system coincides with the smallest nonlinear contributions to C (cf. Fig. 1 vs. Fig. 7D).

6.2. Model Predictions

Our intent is to create a chemical model that captures the full rheological behaviour of melts in the system Di-An-Ab using the basic VFT equation (Eqn. 1). This requires the model to predict the temperature dependence (Arrhenian and non-Arrhenian) of melt viscosity across the full compositional range of the Di-An-Ab ternary system. Furthermore, an effective model is one that accommodates the pronounced changes in rheology that can arise from relatively small, continuous changes in melt composition or temperature.

We illustrate the power of this model by plotting model VFT functions for a variety of melt compositions across the temperature range 900 to 2500 K (≅625–2225°C; Fig. 8). VFT functions are plotted for individual melt compositions at 10 mol% increments along each of the binaries (Fig. 8A–C). Melts from the Di-An binary (Fig. 8A) all show relatively fragile (e.g., non-Arrhenian) rheological behaviour. At high temperatures, melt viscosity along the join varies by <1 log unit, whereas at lower temperature ($<$1000 K) the variation in viscosity is >7 orders of magnitude.

The model VFT functions for melts along the Ab-An binary show quite a different pattern. These melts span the full range of behaviour, from strong (Ab) to fragile (An), and

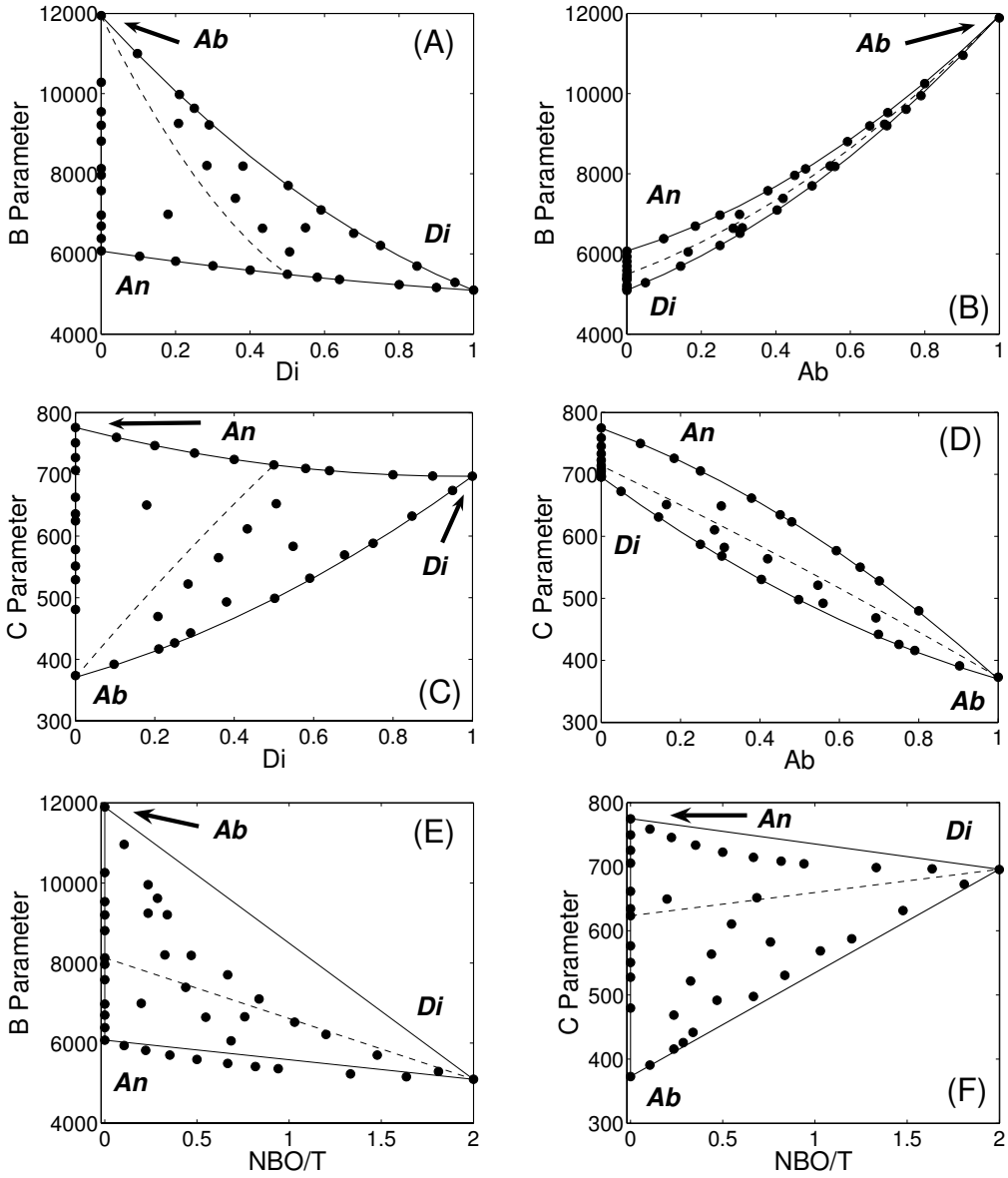

Fig. 6. Values of B and C calculated with multicomponent model for melts in system Di-An-Ab plotted against compositional parameters: (A) B vs. X_{Di}; (B) B vs. X_{Ab}; (C) C vs. X_{Di}; (D) C vs. X_{Ab}; (E) B vs. NBO/T; and (F) C vs. NBO/T. Solid circles are values of B and C computed for compositions in original experimental database. Solid lines show values of B and C for melts on binaries; dashed line shows values for melt compositions $Di_xAn_xAb_{1-2x}$.

intermediate melts have intermediate properties. The consequence of this is an important crossover in viscosity as a function of temperature. At high temperatures in the interval 1250 to 2500 K, Ab and Ab-rich melts always have the highest viscosity. Below 1200 K, An and An-rich melts have higher viscosity. This behaviour is also found in natural melts between rhyolite (e.g., Ab) and basalt (e.g., An; Giordano and Dingwell, 2004). Melts along the join Di-Ab also involve a strong (Ab) and more fragile (Di) end member, but define yet another pattern in VFT functions. At high temperatures these melts show a pronounced variation in viscosity with composition (≅3 log units at 2500 K). With increasing Di content, these melts move gradationally to lower values of viscosity. This behaviour is consistent at temperatures in excess of 1100 K. However, below 1100 K a weak crossover develops whereby Di and Di-rich melts have higher viscosities than some of the more Ab-rich melts.

We have also plotted the model VFT functions for melt compositions having equal proportions of An:Ab (Fig. 8D), Di:Ab (Fig. 8E), and Di:An (Fig. 8F). VFT curves are calculated for melts at increasing increments (e.g., 10 mol%) of the third component. For melts having equal proportions of An and Ab, increasing x_{Di} causes a gradual decrease in melt viscosity (Fig. 8D). The only aberration is at temperatures below 1000 K where there is a minor crossover involving Di-rich melts. A quite different pattern emerges for melts having equal Di-Ab contents (Fig. 8E). Regardless of the An content, these melts show essentially uniform values of Arrhenian-like viscosity

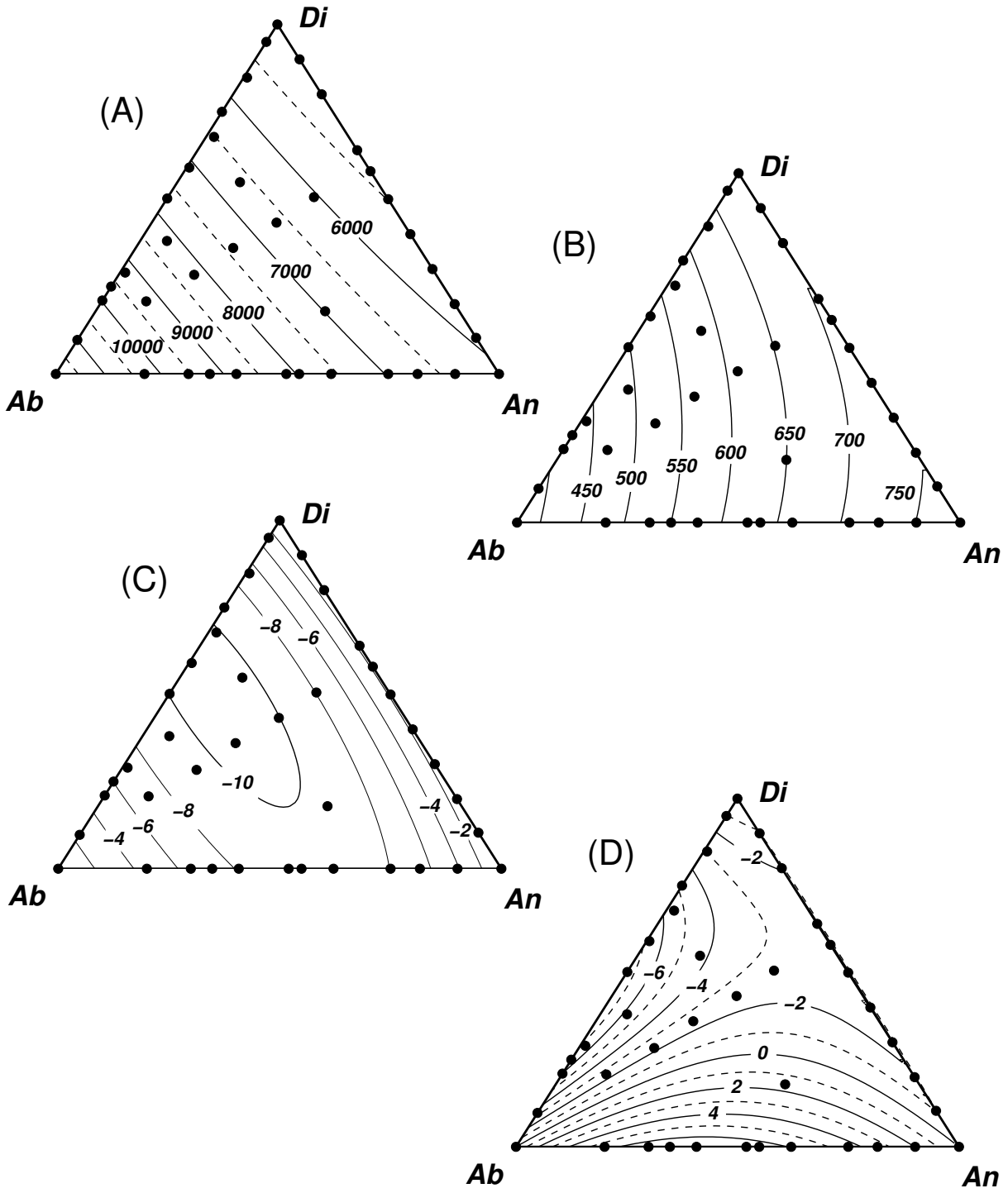

Fig. 7. Model variations in B and C across the system Di-An-Ab. Ternary system contoured for: (A) values of B; (B) values of C; (C) nonlinear compositional component (%) of B; and (D) nonlinear compositional component (%) of C.

over the temperature interval 1500 to 2500 K. Below this temperature the melts show strongly non-Arrhenian behaviour, and the effect of An-content is to increase viscosity at constant temperature. At 1150 K, the apparent values of viscosity across this system vary by at least 6 orders of magnitude. The last system features equal proportions of An and Di and increasing Ab content (Fig. 8F). The pattern that emerges is very similar to that shown in Figure 8C for Ab-Di melts; this reflects the fact that the viscosity of Di and An melts has similar temperature dependencies (Fig. 8A).

The measure of a model is its capacity to reproduce and explain the data used in its calibration and to make predictions

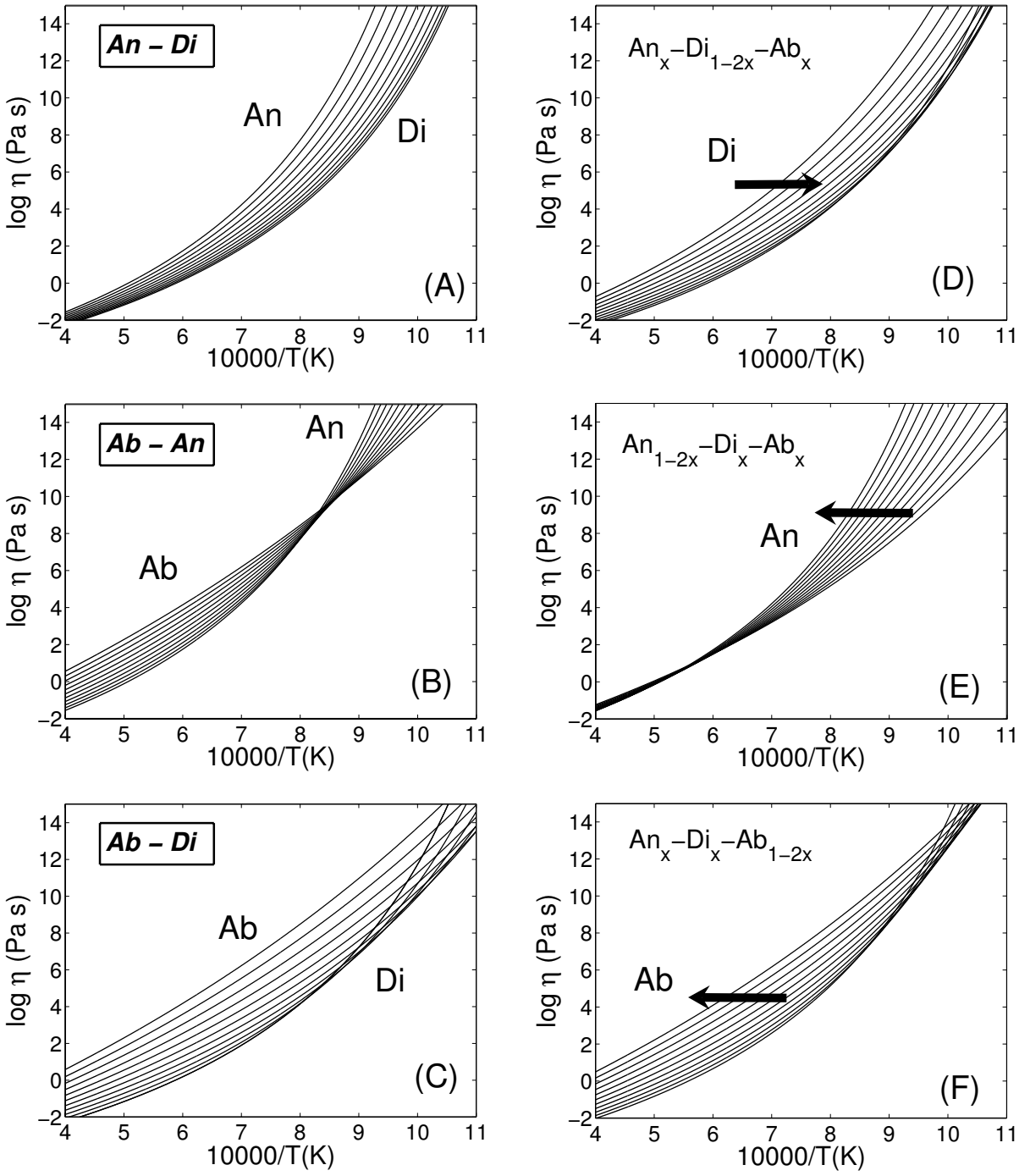

Fig. 8. Model VFT functions showing temperature dependence of melt viscosity in system Di-An-Ab for specific melt compositions, including (A) binary An-Di at intervals of X_{Di} of 0.1; (B) binary Ab-An at intervals of X_{An} of 0.1; (C) binary Ab-Di at intervals of X_{Di} of 0.1; (D) An_x-$Di_{1-2x;}$-Ab_x; (E) An_{1-2x}-Di_x-Ab_x; and (F) An_x-Di_x-Ab_{1-2x}.

beyond the original data set. As discussed earlier, there are portions of the Di-An-Ab ternary system for which there are no reliable viscosity data (Fig. 1). To demonstrate the capacity of this model for extrapolation, we selected representative compositions from several domains where data are scarce (Fig. 1; Table 5). The predicted viscosity-temperature relationships for these melts are compared to the few experiments that are available.

We did not use the viscosity data for the melt $Di_{13.1}An_{30.6}Ab_{54.3}$ from Tauber (1987) to calibrate our model because there was a 4 mol% Ab discrepancy between the nominal and measured composition of the melt. Here we have used the reported composition (wt% oxides; Tauber, 1987) to compute the model VFT parameters and corresponding viscosity: T(K) properties of the melt (Table 5). The comparison between model and data (solid dots, Fig. 9) is within the

Table 5. Predicted values of B and C for melt compositions not used to calibrate model (Fig. 1) and their calculated values of Tg and fragility.

Sample	No. 23	No. 14	No. 5	No. 5[1]	No. 5[2]
Source	Tauber (1987)	Kozu and Kani (1935)	Kozu and Kani (1935)	—	—
Di	13.1	20	60	60.2	59.8
An	30.6	60	20	20.1	19.9
Ab	54.3	20	20	17	22.9
A	−5.06	−5.06	−5.06	−5.06	−5.06
B	8253.4	6514.5	6112.6	5840.4	6377.9
C	544.3	682.9	626.1	618.6	633.3
Tg (K)	1028	1065	984	961	1007
F_D	0.53	0.64	0.64	0.64	0.63
F_m	36.3	47.6	46.9	47.9	46
$F_{1/2}$	0.36	0.47	0.47	0.48	0.46

Composition No. 5 was modified by reducing [1] or increasing [2] Na_2O by 0.4 wt%.

uncertainty of the viscosity measurements and is very good if the vagaries of melt composition are considered. The data of Kozu and Kani (1935) were not included in our model because the compositions of experimental melts were not measured independently. We have computed the model VFT functions for these two melts using the reported nominal compositions (Table 5). The data for the melt $Di_{20}An_{20}Ab_{20}$ cover only a small range of temperatures (open triangles, Fig. 9), but are well described by the model VFT function. We also reproduce the viscosity measurements for $Di_{60}An_{20}Ab_{20}$ (Kozu and Kani, 1935) in that the model curve goes through the middle of the data set and parallels the low-T measurements (crosses, Fig. 9). The shaded field denotes the area covered by a family of VFT functions resulting from adding or subtracting up to 0.4 wt% Na_2O to the nominal composition (Table 5). The dispersion in the Kozu and Kano (1935) data for this melt could have many sources but is easily explained by small differences between the nominal and actual Na_2O contents of the melt.

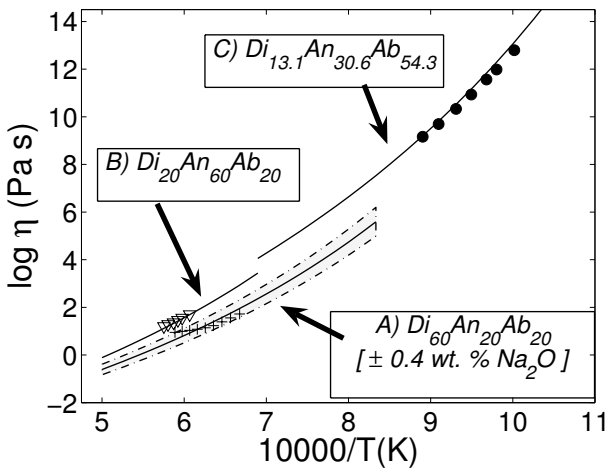

Fig. 9. Prediction of viscosity for specific melt compositions not used to calibrate model (see Fig. 1) and compared to experimental data. (A) $Di_{60}An_{20}Ab_{20}$; (B) $Di_{20}An_{60}Ab_{20}$; and (C) $Di_{13.1}An_{30.6}Ab_{54.3}$ (see Table 5). Dashed lines contain the family of VFT curves predicted for the melt $Di_{60}An_{20}Ab_{20}$ and accounts for variations in Na_2O contents of ±0.4 wt%.

6.3. Implications

This chemical model for melt viscosity represents an empirical parameterization of the VFT equation for the effects of composition; it uses no theoretical basis for assigning compositional dependence to the adjustable parameters (e.g., A, B, and C). In particular, the component basis we used was adopted for convenience (e.g., over simple oxides) after restricting the model to strictly ternary (e.g., Di-An-Ab) melt compositions. This basis is perfectly adequate for the mathematical description of the compositional dependence of viscosity. However, these components are not intended to be (and are unlikely to be) representative of the structural units (e.g., speciation) in the melt that mix and control variations in melt viscosity. This choice of components also restricts the model's capacity for extrapolation out of the strictly ternary system. The chemical model does, however, provide a vehicle for exploring the implicit role of composition on other melt properties, including the glass transition temperature (T_g; e.g., Angell, 1997; Toplis et al., 1997; Toplis, 1998) and melt fragility (e.g., Angell, 1985; Angell, 1991; Rossler et al., 1998; Giordano and Dingwell, 2003b).

6.3.1. *Glass transition temperatures*

Conventionally, a measure of T_g is given by the temperature at which a melt achieves a viscosity of 10^{12} Pa s (e.g., Richet and Bottinga, 1995; Webb and Knoche, 1996; Sipp et al., 2001). We have used our viscosity model to calculate the corresponding values of T_g for melt compositions across the Di-An-Ab ternary system (Table 4):

$$T_g = C + \frac{B}{12 - A} \quad (7)$$

where B and C vary with the composition of the melt. Results are summarized in Figure 10, where model values of T_g are plotted against the mole fraction of Di, Ab, and An and by contouring the ternary for values of T_g (Fig. 10D).

The highest model value of T_g corresponds to An (1131 K). The minimum T_g value (947 K) does not coincide with an end-member melt composition, but occurs on the Di-Ab binary at ≅60 mol% Di (Fig. 10A–D). Values of T_g change nonlin-

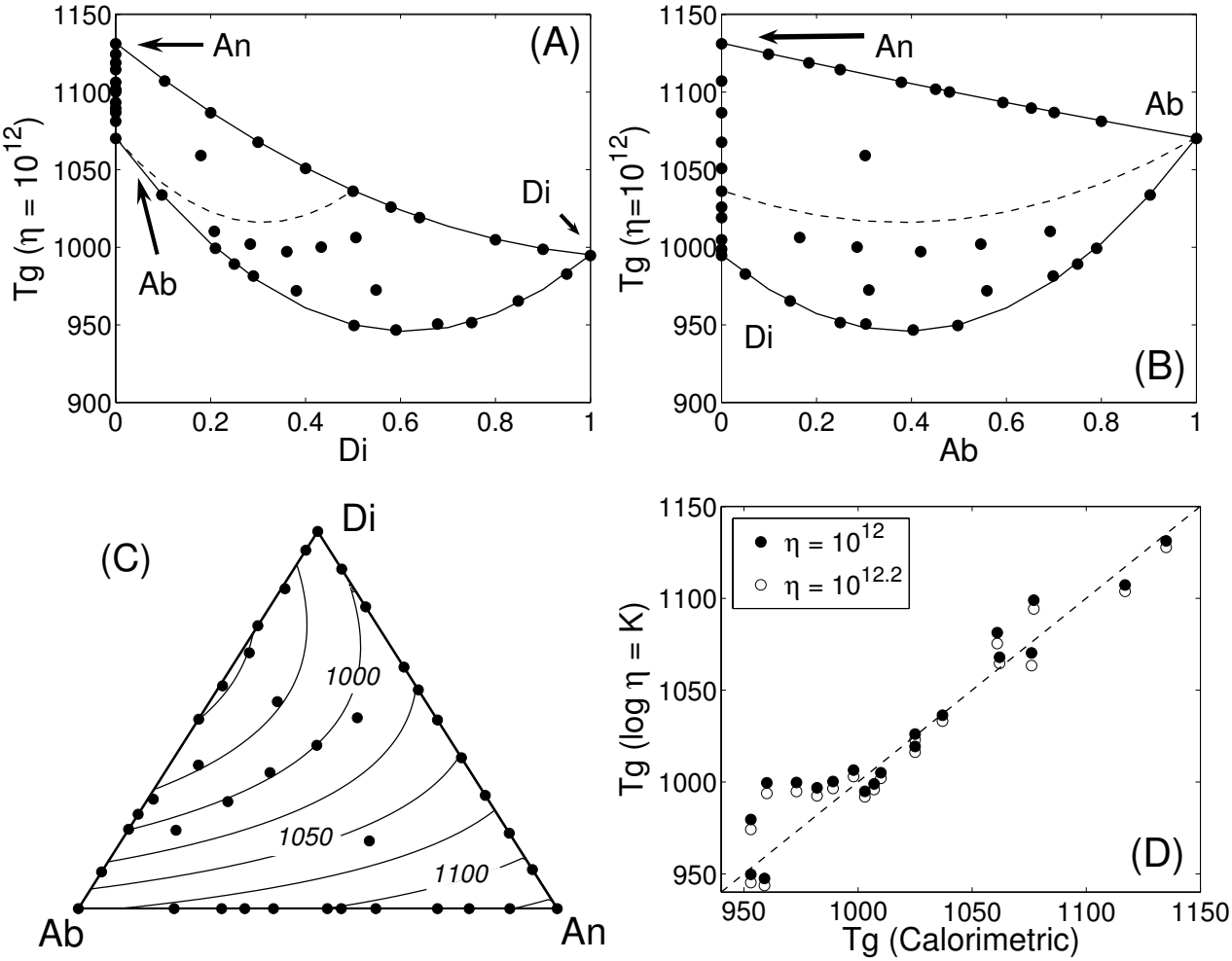

Fig. 10. Calculated glass transition temperatures (T_g) across system Di-An-Ab defined as the temperature where melt viscosity equals 10^{12} Pa s. T_g plotted against (A) X_{Di} and (B) X_{Ab}. Lines in (A) and (B) are as in Figure 6. (C) Ternary system contoured for values of T_g. (D) Calorimetric values of Tg (Webb and Knoche, 1996) for Di-An-Ab melts are compared to T_g values predicted by this model for $\eta = 10^{12}$ or $10^{12.2}$ Pa s (see text).

early with increasing Di content along both the Di-An and Di-Ab joins (Fig. 10A). T_g values along the Di-An binary are always lower than the T_g values associated with the end members. This depression in apparent T_g values is even more pronounced (up to ≅90°C) along the Di-Ab binary (Fig. 10A,B). In contrast, values of T_g decrease linearly with increasing Ab content along the binary An-Ab (Fig. 10B,C). The T_g values for ternary melt compositions are also depressed relative to T_g values of the end-member melt compositions. This implies that values of T_g along the binaries or within the ternary cannot simply be predicted using the T_g values for the end-member melt compositions.

The predicted values of T_g for the end-member melt compositions (Di, An, Ab) are 994 K, 1131 K, and 1070 K. These values agree well with calorimetric measurements of T_g for the end-members Di (1003–1009 K), An(1135–1143 K), and Ab (978–1076 K) based on a cooling/heating rate of 5 K/min(Webb and Knoche, 1996). Figure 10D shows explicitly the relationship between the calorimetric T_g values measured by Webb and Knoche (1996) and those calculated by our model at a viscosity of 10^{12} Pa s. We have made the comparison for 20 of the ternary melt compositions reported by Webb and Knoche (1996). We excluded several compositions which showed discrepancies between the nominal and measured composition (e.g., several glasses from Tauber, [1987]). In such instances, we are unable to predict T_g ($\eta \approx 10^{12}$ Pa s) accurately because the calculated values of B and C might be for compositions different from those measured by Webb and Knoche (1996).

Figure 10D shows excellent agreement between the calorimetric T_g's and the values predicted by our model. This coincidence suggests that, for these melts at least, the timescale of thermal relaxation during the calorimetric experiment (5K/min) is matched by the characteristic relaxation timescale of melts at 10^{12} Pa s. Calorimetric measurements performed at a more rapid cooling/heating rate would result in higher values of T_g and would only match the rheological T_g's corresponding to the faster characteristic relaxation timescales found at lower viscosities. We can improve on this comparison by solving for the optimal η_{Tg} to best match the calorimetric Tg values of Webb and Knoche (1996). This is achieved by entering the calorimetric Tg into Eqn. 7 with

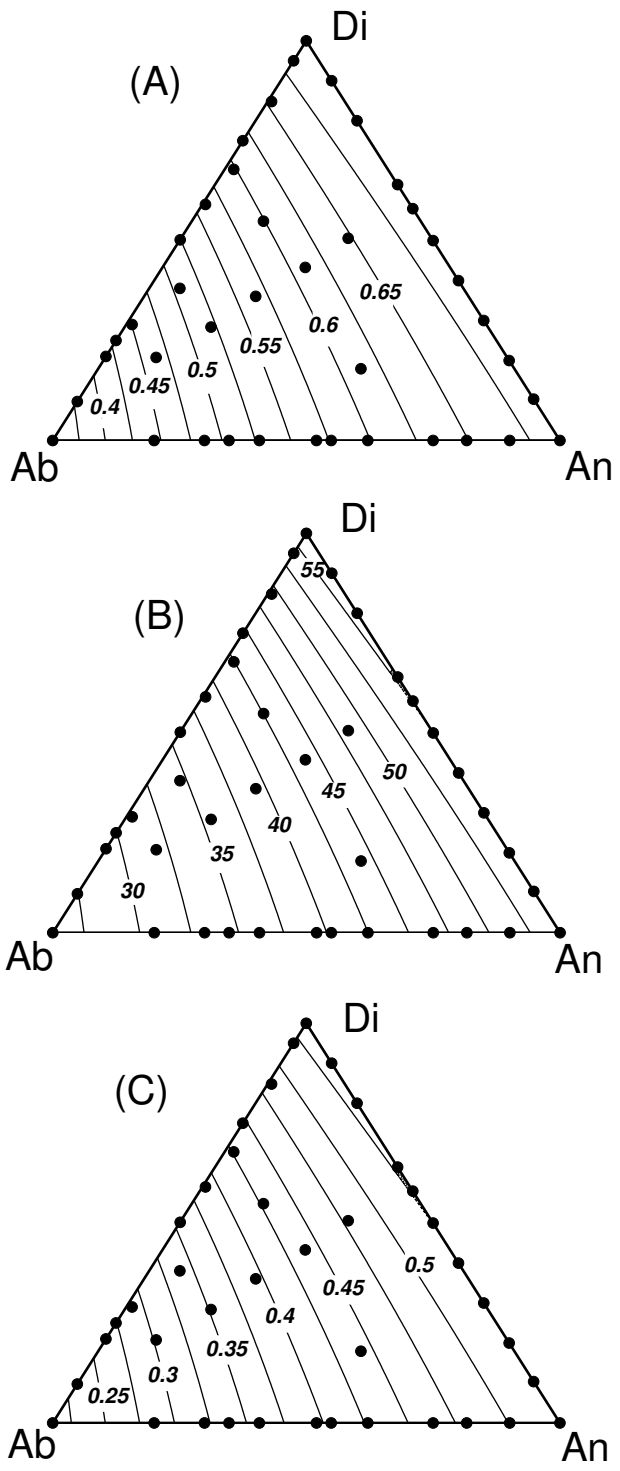

Fig. 11. Calculated indices for melt fragility in system Di-An-Ab and summarized as contour plots (see text). Contoured values of (A) fragility (F_D = C/B), (B) steepness index (m = B/[T_g (1-C/T_g)^2]), and (C) $F_{1/2}$ fragility ($F_{1/2}$ = 2[T_g/$T_{1/2}$ - 0.5]).

the appropriate values of A (-5.06), B, and C for each melt composition. Solving the system of equations for η_{Tg} returns a value of $10^{12.2\pm0.1}$ Pa s (open circles, Fig. 10D).

6.3.2. Melt fragility

The viscosity model can also be used to compute several indices for melt fragility (Table 4). Fragility (F) was a concept developed by Angell (1985) to distinguish two extreme behaviours of glass-forming liquids: *strong* (Arrhenian-like) and *fragile* (non-Arrhenian). Values of fragility can be calculated from the adjustable parameters in the VFT equation: F_D = C/B (F_D = D^{-1} as developed by Angell, 1985; Angell, 1991). Low values of F correspond to strong liquids, whereas high F values correspond to fragile liquids. The strong/fragile classification is used to compare the sensitivity of liquid structure to temperature changes. Melts that are fragile easily assume a large variety of configurational states in response to thermal perturbations; strong liquids resist structural change, even if subjected to large temperature variations. An alternative method of ranking strong to fragile liquids is the steepness index (*m*), which is calculated as B/[T_g (1 - C/T_g)^2] (e.g., Plazek and Ngai, 1991; Böhmer and Angell, 1992; Rossler et al., 1998). Essentially, the steepness index (*m*) represents the derivative of log η with respect to the reduced temperature at T_g. A third and final method of classifying strong and fragile melts is based on the $F_{1/2}$ fragility index (e.g., Richert and Angell, 1998; Martinez & Angell, 2001), which is computed as $F_{1/2}$ = 2[T_g/$T_{1/2}$ - 0.5] where T_g is as defined above (see Table 4) and $T_{1/2}$ is the temperature at the half way point (log scale) between the high temperature relaxation time limit and Tg where τ = 10^2 s. Given our best estimate of A (-5.06), the Maxwell relationship suggests a high temperature relaxation time limit of 10^{-15} s, and thus, $T_{1/2}$ is the temperature corresponding to a viscosity of $10^{3.5}$ Pa s (Table 4).

All three fragility indices have been computed for the full range of compositions within the Di-An-Ab ternary system (Table 4; Fig. 11). The contoured plots for each index show that, although the numerical values differ (F_D: 0.35–0.7; *m*: 26–57; $F_{1/2}$: 0.2–0.55), the three different indices provide the same insights. The strongest melt (lowest fragility index) is Ab, and the most fragile melt is Di, although An is only slightly less fragile. The contoured plots show a smooth gradual rise in fragility index from Ab to Di and An; indeed the contours closely parallel the Di-An join. The fragility of binary and ternary melts can be directly predicted from the fragility indices of the Di, An, and Ab alone. Fragility indices for mixtures in this system are linear combinations of the end members. This is in stark contrast to predicted values of Tg where binary and ternary melt compositions are substantially depressed relative to the end member properties.

7. CONCLUSIONS

We have presented a chemical model for the compositional and temperature dependence of melt viscosity in the ternary system Di-An-Ab. Temperature dependence of melt viscosity was ascribed to the VFT equation which features three adjustable parameters: A, B, and C. We assume that all silicate melts converge to a common viscosity at high temperature, which makes A independent of composition. All compositional dependence is therefore embedded in the parameters B and C; the compositional dependence of these parameters involves a linear and a higher order, nonlinear component. Optimal values for the 13 parameters (A, $b_{i=1,2..6}$, $c_{j=1,2..6}$) are obtained by solving

a system of equations based on 585 experimental measurements of viscosity on 40 different melt compositions.

The best estimate for A is −5.06, which implies a high-temperature limit to viscosity (η_0) of $10^{-5.06}$ Pa s. This value accords well with several other lines of inquiry. For example, a high-T limit to melt viscosity is implicit to Shaw's (1972) Arrhenian model for silicate melt viscosities and is given by ln η_0 (poise) = -(1.5 M + 6.4), where M is a composition-dependent variable. For a wide range of melt compositions, the range of high-T viscosity values converge to 10^{-5} to 10^{-6} Pa s. Our result of $\eta_0 = 10^{-5.06}$ Pa s is also supported by experimental observations on lower temperature glass-forming systems (e.g., Angell, 1991; Angell et al., 2000) and theoretical arguments involving Maxwell's relationship ($\tau = \eta/G_\infty$) applied to timescales of relaxation processes in melts (e.g., Glasstone et al., 1941; Myuller, 1955; Frenkel, 1959; Dingwell and Webb, 1989; Toplis 1998; Angell et al., 2000).

The optimization returns 12 coefficients that capture the compositional dependence of B and C. The compositional dependence of B and C is almost linear except for a 10 and 7% nonlinear component in each, respectively. Taken together, the 13 parameters listed in Table 3 constitute a model that can generate accurate VFT functions for melts across the Di-An-Ab system. The model is continuous and accommodates marked changes in rheology with composition. Despite the near-linear compositional dependence of B and C, the model is capable of reproducing the pronounced nonlinearities exhibited by the original data (e.g., crossing VFT functions for different melt compositions). The model also has a demonstrated capacity for extrapolation beyond the original database.

Acknowledgments—This research was supported by the Natural Sciences and Engineering Research Council of Canada. The senior author received valuable research assistance from Tony Dubin and Kim Munro. Discussions with K.-U. Hess, Don Dingwell, and Greg Dipple have helped focus many of our ideas. D. Giordano acknowledges the postdoctoral fellowship support from the Dorothy Killam Trust administered by The University of British Columbia. The manuscript benefited from critical and thoughtful reviews from three anonymous referees.

REFERENCES

Angell C. A. (1985). Strong and fragile liquids. In *Relaxations in Complex Systems.* (ed. K. L. Ngai and G. B. Wright) pp. 3–11, U.S. Department of Commerce National Technical Information Service.

Angell C. A. (1991) Relaxation in liquids, polymers and plastic crystals - strong/fragile patterns and problems. *J. Noncryst. Solids* **131–133**, 13–31.

Angell C. A. (1997) Entropy and fragility in supercooled liquids. *J. Res. NIST* **102,** 171–185.

Angell C. A., Ngai K. L., McKenna G. B., McMillan P. F., and Martin S. W. (2000) Relaxation in glassforming liquids and amorphous solids. *J. App. Phys.* **88,** 3113–3149.

Baker D. R. (1996) Granitic melt viscosities: Empirical and configurational entropy models for their calculation. *Am. Mineral.* **81,** 126–134.

Böhmer R. and Angell C. A. (1992) Correlations of the nonexponentiality and state dependence of mechanical relaxations with bond connectivity in Ge-As-Se supercooled liquids. *Phys. Rev.* **45,** 10091–10094.

Bottinga Y. and Weill D. (1972) The viscosity of magmatic silicate liquids: a model for calculation. *Am. J. Sci.* **272,** 438–475.

Bottinga Y., Richet P., and Sipp A. (1995) Viscosity regimes of homogeneous silicate melts. *Am. Mineral.* **80,** 305–319.

Brearley M., Dickinson J. E. Jr., and Scarfe C. M (1986) Pressure dependence of melt viscosity on the join diopside-albite. *Geochim. Cosmochim. Acta* **50,** 2563–2570.

Cranmer D. and Uhlmann D. R. (1982) Viscosities in the system albite-anorthite. *J. Geop. Res.* **86,** 7951–7956.

Dingwell D. B. (1995) Relaxation in silicate melts: Applications. In *Structure, Dynamics and Properties of Silicate Melts* (eds. J. F. Stebbins, P. F. McMillan and D. B. Dingwall) *Reviews in Mineralogy* **32,** 21–66.

Dingwell D. B. and Webb S. L. (1989) Structural relaxation in silicate melts and nonNewtonian melt rheology in geologic processes. *Phys. Chem. Minerals.* **16,** 508–516.

Frenkel Y. I. (1946) *Kinetic Theory of Liquids*. Clarendon Press, Oxford.

Fulcher G. S. (1925) Analysis of recent measurements of the viscosity of glasses. *J. Am. Ceramic Soc.* **8,** 339–355.

Giordano D. and Dingwell D. B. (2003a) Non-Arrhenian multicomponent melt viscosity: a model. *Earth Planet. Sci. Lett.* **208,** 337–349.

Giordano D. and Dingwell D. B. (2003b) The kinetic fragility of natural silicate liquids. *J. Phys. Condens. Matter 15*, S945–S954.

Giordano D., Romano C., Papale P., and Dingwell D. B. (2004) The viscosity of trachytes, and comparison with basalts, phonolites and Rhyolites. *Chem. Geol.* **213,** 49–61.

Glasstone S., Laidler K., and Eyring H. (1941). *Theory of Rate Processes.* McGraw-Hill.

Hess K. U. and Dingwell D. B. (1996) Viscosities of hydrous leucogranitic melts: A non-Arrhenian model. *Am. Mineral.* **81,** 1297–1300.

Hess K. U., Dingwell D. B., and Rossler E. (1996) Parameterization of viscosity-temperature relations of aluminosilicate melts. *Chem. Geol.* **128,** 155–163.

Hummel W. and Arndt J. (1985) Variation of viscosity with temperature and composition in the plagioclase system. *Contrib. Mineral. Petrol.* **90,** 83–92.

Kirkpatrick R. J. (1974) Kinetics of crystal growth in the system $CaMgSi_2O_6$-$CaAl_2SiO_6$. *Am. J. Sci.* **274,** 215–242.

Kozu S. and Kani K. (1935) Viscosity measurements of the ternary system diopside-albite-anorthite at high temperatures. *Imperial Acad. Japan (Tokyo) Proc.* **11,** 383–385.

Kushiro I. (1978) Viscosity and structural changes of albite ($NaAlSi_3O_8$) melt at high pressures. *Earth Planet. Sci. Lett.* **41,** 87–90.

Licko T. and Danek V. (1986) Viscosity and structure of melts in the system CaO-MgO-SiO_2. *Physics Chem. Glasses* **27,** 22–26.

Machin J. S. and Tin B. Y. (1954) Viscosity studies of system CaO-MgO-Al_2O_3-SiO_2: IV, 60 and 65% SiO_2. *J. Am. Ceram. Soc.* **37** (*4*), 177–186.

Machin J. S., Tin B. Y., and Hanna D. L. (1952) Viscosity studies of system CaO-MgO-Al_2O_3-SiO_2: III, 35, 45 and 50% SiO_2. *J. Am. Ceram. Soc.* **35** (*12*), 322–325.

Martinez L. M. and Angell C. A. (2001) A thermodynamic connection to the fragility of glass-forming liquids. *Nature* **410,** 663–667.

Mysen B. O. (1986) Structure and petrologically important properties of silicate melts relevant to natural magmatic liquids. In *Short Course on Silicate Melts* (ed. C. M. Scarfe), pp. 180–209, Mineralogical Association of Canada.

Mysen B. O., Virgo D., and Seifert F. A. (1982) The structure of silicate melts: implications for chemical and physical properties of natural magma. *Rev. Geophys. Space Phys.* **20,** 353–383.

Myuller R. L. (1955) A valence theory of viscosity and fluidity for high-melting glass-forming materials in the critical temperature range. *Zh. Prikl. Khim.* **28,** 1077–1087.

N'Dala I., Cambier F., Anseau M. R., and Urbain G. (1984) Viscosity of liquid feldspars- Part I: Viscosity measurements. *Br. Ceram. Trans. J.* **83,** 105–107.

Neuville D. R. and Richet P. (1991) Viscosity and mixing in molten (Ca, Mg) pyroxenes and garnets. *Geochim. Cosmochim. Acta* **55,** 1011–1019.

Persikov E. S. (1991) The viscosity of magmatic liquids: experiment generalized patterns, a model for calculation and prediction, applications. In *Physical Chemistry of Magmas, Advances in Physical Chemistry* (ed. L.L. Perchuk and I. Kushiro), pp. 1–40, Springer.

Persikov E. S. (1998) Viscosities of model and magmatic melts at the pressures and temperatures of Earth's crust and upper mantle. *Russian Geology and Geophysics* **39,** 1780–1792.

Plazek D. J. and Ngai K. L. (1991) Correlation of polymer segmental chain dynamics with temperature-dependent time-scale shifts. *Macromolecules* **24,** 1222–1224.

Press W. H., Flannery, B. P., Teukolsky, S. A., and Vetterling, W. T (1986) *Numerical Recipes: The Art of Scientific Computing.* Cambridge University Press.

Prusevich A. A. (1988) Refinement of calculation of viscosity of magmatic melts according to their chemical composition. *Geologiya i Geofizika* **29,** 67–69.

Richert R. and Angell C. A. (1998) Dynamics of glass-forming liquids. V. On the link between molecular dynamics and configurational entropy *J. Chem. Phys.* **108,** 9016–9026.

Richet P. and Bottinga Y (1995) Rheology and configurational entropy of silicate melts. In *Structure, Dynamics and Properties of Silicate Melts,* Reviews in Mineralogy, Vol. 32 (ed. J. F. Stebbins, P. F. McMillan, and D. B. Dingwell), pp. 67–93, Mineralogical Society of America.

Rossler E., Hess K. U., and Novikov V. N. (1998) Universal representation of viscosity in glass forming liquids. *J. Noncryst. Solids* **223,** 207–222.

Russell J. K., Giordano D., Dingwell D. B., and Hess K. U. (2002) Modelling the non-Arrhenian rheology of silicate melts: Numerical considerations. *Eur. J. Mineral.* **14,** 417–427.

Russell J. K., Giordano D., and Dingwell D. B. (2003) High-temperature limits on viscosity of non-Arrhenian silicate melts. *Am. Mineral.* **88,** 1390–1394.

Scarfe C. M. and Cronin C. J. (1986) Viscosity-temperature relationships of melts at 1 atm in the system diopside-albite. *Am. Mineral.* **71,** 767–771.

Scarfe C. M., Cronin D. J., Wenzel J. T., and Kaufman D. A. (1983) Viscosity-temperature relationships at 1 atmosphere in the system diopside-anorthite. *Am. Mineral.* **68,** 1083–1088.

Schulze F., Behrens H., and Hurkuck W. (1999) Determination of the influence of pressure and dissolved water on the viscosity of highly viscous melts: Application of a new parallel-plate viscometer. *Am. Mineral.* **84,** 1512–1520.

Shaw H. R. (1972) Viscosities of magmatic silicate liquids: An empirical model of prediction. *Am. J. Sci.* **272,** 438–475.

Sipp A., Bottinga Y., and Richet P. (2001) New high viscosity data for 3D network liquids and new correlations between old parameters. *J. Noncryst. Solids* **288,** 166–174.

Spera F. J. (2000) Physical properties of magma. In *Encyclopedia of Volcanoes* (ed. H. Sigurdsson), pp. 171–190, Academic Press.

Stein D. J. and Spera F. J. (1993) Experimental rheometry of melts and supercooled liquids in the system $NaAlSiO_a$-SiO_2: Implications for structure and dynamics. *Am. Mineral.* **78,** 710–723.

Sykes D., Dickinson J. E.,. Luth R. W., and Scarfe C. M. (1993) Viscosity-temperature relationships at 1 atm in the system nepheline-diopside. *Geochim. Cosmochim. Acta* **57,** 1291–1295.

Tammann G. and Hesse W. (1926) Die Abhängigkeit der viskosität von der temperatur bei unterkühlten flüssigkeiten. *Zeitschrift für Anorganische und Allgemeine Chemie* **156,** 245–257.

Taniguchi H. (1992) Entropy dependence of viscosity and the glass transition temperature of melts in the system diopside-anorthite. *Contrib. Mineral. Petrol.* **109,** 295–303.

Tauber P. (1987) *Viskositätsuntersuchungen in Modellsystem Anorthit-Albit-Diopsid.* Dissertation, Univeristät Tubingen.

Tauber P. and Arndt J. (1987) The relationship between viscosity and temperature in the system Anorthite–Diopside. *Chem. Geol.* **62,** 71–81.

Toplis M. J. (1998) Energy barriers to viscous flow and the prediction of glass transition temperatures of molten silicates. *Am. Mineral.* **83,** 480–490.

Toplis M. J., Dingwell D. B., Hess K. U., and Lenci T. (1997) Viscosity, fragility and configurational entropy of melts along the join SiO_2-$NaAlSiO_4$. *Am. Mineral.* **82,** 979–990.

Urbain G., Bottinga Y., and Richet P. (1982) Viscosity of silica, silicates and aluminosilicates. *Geochim. Cosmochim. Acta* **46,** 1061–1071.

Vogel D. H. (1921) Temperaturabhängigkeitsgesetz der viskosität von flüssigkeiten. *Physikalische Zeitschrift* **22,** 645–646.

Webb S. R. and Knoche R. (1996) The glass-transition, structural relaxation and shear viscosity of silicate melts. *Chem. Geol.* **128,** 165–183.